16th World Conference on Earthquake, 16WCEE 2017
Santiago Chile, January 9th to 13th 2017
Paper N° 1441 (Abstract ID)
Registration Code: S-H1461548684

Effect of scarp topography on seismic ground motion under inclined P wave

H.P. Ding[1], J. Liao[2], Y.Y. Yu[3], Z.F. Zheng[4]

[1] Professor, Suzhou University of Science and Technology, hpding@126.com
[2] Associate Professor, Suzhou University of Science and Technology, liaojian@126.com
[3] Doctoral student, Suzhou University of Science and Technology, yushunjian1986@126.com
[4] Master student, Suzhou University of Science and Technology, zhengzhifa@126.com

Abstract

The seismic ground motion of a scarp topography under inclined P waves is analyzed using numerical simulation method, and the effects of the incident angle, the slope angle and the incident direction are also discussed. It is shown that: (1) The amplification factor increases gradually from scarp's bottom corner to top corner, and the incident angle, the slope angle and the incident direction have no effect. (2) When the incident angle is a constant, the amplification factor of scarp downside region is greater than that of upside region, regardless of the incident direction, but it increases with the growing of slope angel. (3) When the slope angle is a constant and waves incident from left side, for x component, amplification factor increases with the growing of incident angle, while for z component, the opposite is true. (4) When waves incident from right side, the maximal amplification factor is generally at top corner of scarp. If incident direction is reverse, the maximal amplification factor departs from the top corner, and the larger the slope angle, the greater the deviation. (5) When waves incident from left side, the x component amplification factor is larger compared with right incidence case, but z component amplification factor is not sensitive to the incident direction.

Keywords: scarp topography; inclined P wave; ground motion; amplification factor

1. Introduction

Topography has important influence on seismic ground motion. It is often found that earthquake damage at the mountain ridges, the escarpments, the high isolated hills, and the edge of scarp or slope is obviously severe. For instance, in 1966 Dongchuan, Yunnan earthquake, damage of a convalescent hospital, which was located at the upper edge of a hill, was more severe than that of the base. Besides, in 1970 Tonghai, Yunnan earthquake, villages located at the regional raised hills or ridges suffer more intensive destructions than the surrounding area. And in 1988 Lancang-Gengma, Yunnan earthquake, some multi-storey buildings at the top of isolated hills were destroyed, whereas the one storey houses almost had no damages[1]. The seismic records also show these characteristics. Using the aftershock records of the San Fernando earthquake, Davis and West (1973) found that accelerations at the mountaintop were several times larger compared with that at the mountain base[2]. The observed velocity records at the crest and base of Kagel Mountain showed that the duration time of seismic motion at the crest increased obviously, accompanying with significant amplification effects[3]. In 2008 Wenchuan earthquake, the records of the strong motion observatory array deployed at Zigong Xi-shan Park showed that the PGA values of 7 bedrock stations generally increase from mountain base to top[4].

Besides field experiments, the analytical and numerical methods are another two main means to study the effect of topography on seismic ground motion. The analytical methods are mainly used in response studying of regular topographies, such as the semi-cylindrical and semi-elliptical canyons[5-6], the semi-cylindrical and semi-elliptical alluvial valleys[7-8], shallow circular cylindrical canyons[9], circular-arc shaped cylindrical canyon[10], and shallow circular alluvial valleys[11] under incident plane SH waves; the semi-circular canyons under incident plane P waves[12], etc. However, for irregular topography such as scarps, the analytical methods are not suitable, and the numerical methods are often used, which mostly follows a vertical incidence assumption. In contrast, the oblique incidence conditions get much less studies.Ashford and Sitar[13-14] investigated three parameters to quantify the topographic effects of steep slopes under inclined SH waves, i.e., the topographic amplification $A_t = (a_{\max} - a_{ffc}) / a_{ffc}$, the site amplification $A_s = (a_{ffc} - a_{fft}) / a_{fft}$, and the apparent amplification $A_a = (a_{\max} - a_{fft}) / a_{fft}$, where a_{fft} is the maximum free-field acceleration in front the toe, a_{ffc} is the maximum free-field acceleration behind the crest, and $a_{\max}$ is the maximum crest acceleration.

In this study, numerical simulation method combining the finite element method and the multi-transmitting boundary condition is applied to investigate the effects of scarp topography under inclined P waves, and emphasis is put on the influence of the incident angle θ, the slope angle α, and the incident direction on the seismic wave propagation and amplification behavior.

2. Calculation method and model

2.1 Calculation method

In the topographic effect study under inclined seismic waves, the free-field response should be firstly calculated. The free-field motion is also the input motions for the calculation model, which directly affect the simulation accuracy. For the case of obliquely incident seismic waves, the free-field of homogeneous half-space can be determined in time domain by wave propagation rules, and the free-field of layered half-space can be calculated in frequency domain by theoretical method. However, the frequency domain method requires positive and inverse Fourier transforms several times, which makes it time- and storage space- consuming. Zhao et al.[15] proposed an impedance boundary condition based on the relation between stress and velocity on artificial boundary, which improved the simulation accuracy of free field in time domain under inclined P waves. The method of Zhao et al. will be used in this study to calculate the free field, and this time domain method matches the calculation process of two-dimensional finite element method used for the scarp model.

When the finite element method is used in wave motion simulations, the nodes of the computational domain can be divided into internal nodes and artificial boundary nodes. The nodes at the artificial boundaries (referenced as $\boldsymbol{u}_0$ in the following) are artificial boundary nodes, and the other nodes are the internal nodes

(referenced as $\mathbf{u}$ in the following). The nodes at the free surface are the internal nodes. Equation of motion of all the internal nodes is given by

$$\boldsymbol{M}\ddot{\boldsymbol{u}} + \boldsymbol{C}\dot{\boldsymbol{u}} + \boldsymbol{K}\boldsymbol{u} = \boldsymbol{P} \tag{1}$$

where $\boldsymbol{M}$, $\boldsymbol{C}$, and $\boldsymbol{K}$ are the mass, damping, and stiffness matrix, respectively. **P** is the vector of external force, here **P** equals to 0.

The motions of artificial boundary nodes are calculated using the multi-transmitting formula[16-17], that is, the displacement of artificial boundary nodes at time step (p+1) can be obtained by

$$u_0^{p+1} = \sum_{j=1}^{N} (-1)^{j+1} C_j^N u_j^{p+1-j} \tag{2}$$

$$C_j^N = \frac{N!}{(N-j)!\,j!} \tag{3}$$

where *N* is the order of the multi-transmitting formula, *0* denotes the artificial boundary nodes, and *j* represents the internal nodes adjacent to boundary nodes.

It should be noted that the displacement field $\boldsymbol{u}$ in equation (1) is the displacement of full wave field, and the displacement in equation (2) is the displacement of scattered wave field. To the bottom boundary of the calculation model, displacement of scattered wave field can be obtained by subtracting the input wave field from the full wave field. For the side boundaries, displacement of scattered wave field is determined by subtracting the free field from the full wave field.

2.2 Method validation

Considering a homogeneous elastic half space model, the model size and the observation points are shown in Fig.1(a). The P- and S-wave velocities are 866 m/s and 500 m/s, respectively, and the density is 1500 kg/m^3. For the left side boundary, points numbered as 1-16 are equally spaced from point A to point B, with the interval of 20m. For the free surface, points numbered as 16-26 are equally spaced from point B to point C, with the interval of 100m. The displacement time history of the input P wave is shown in Fig.1(b), with a incidence angle $\theta = 60^\circ$. Based on the rule-of-thumb that roughly 6-12 finite elements per minimum wavelength for the FEM, the mesh size is selected as 5 m.

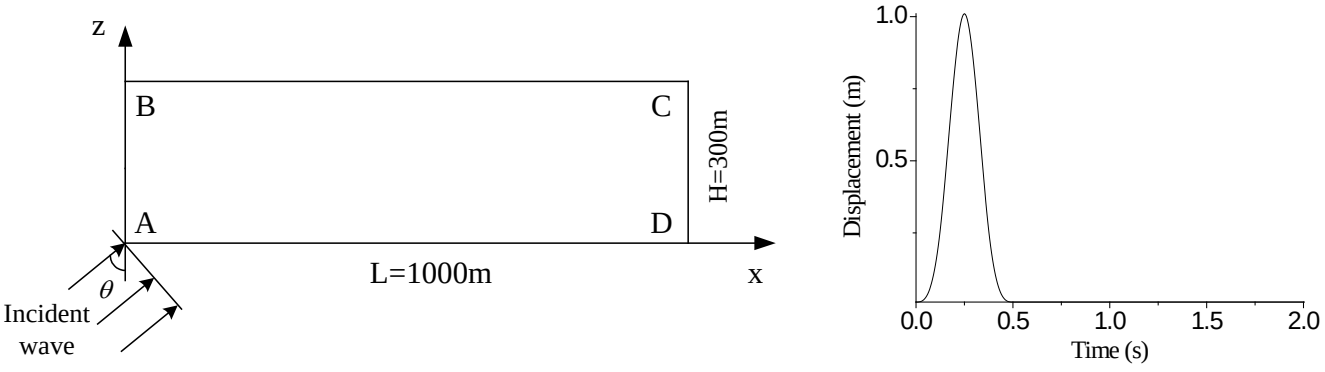

(a) (b)

Fig.1 (a) Calculation model of elastic half-plane; (b) Time history of displacement of incident P wave

The displacement responses of left side and free surface receivers are presented in Fig.2(a) and Fig.2(b), respectively, where the theoretical solution is obtained by the transfer matrix method in frequency domain. It is observed that for the homogeneous elastic half space model, the numerical solutions agree well with the theoretical ones. This implies that the numerical method used in this study is feasible, which calculates the free

field by using the artificial boundary condition proposed in Zhao et al.[15], and simulates the seismic effect of scarp topography by combining the finite element method and the multi-transmitting boundary condition.

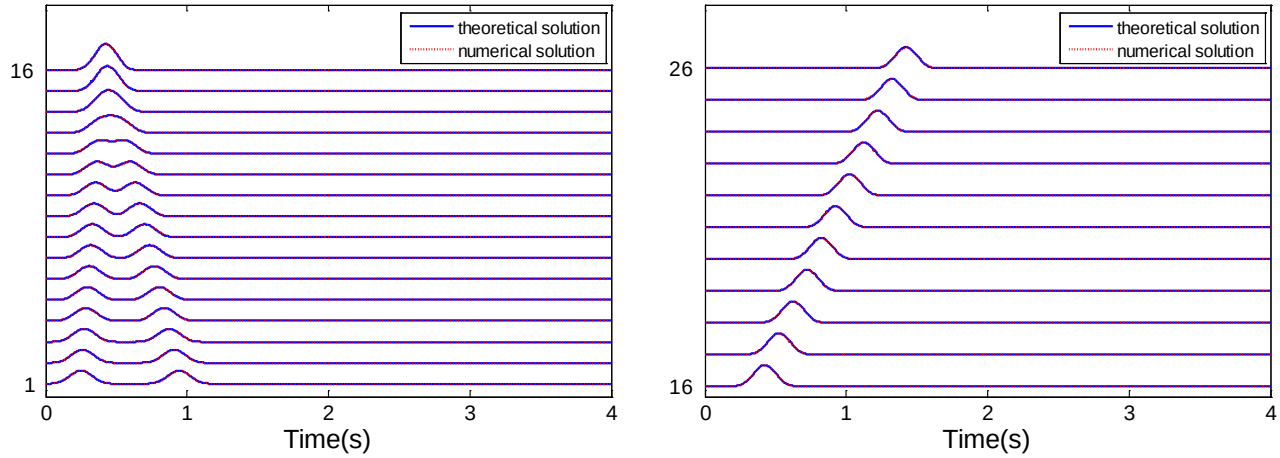

(a) left boundary (b) free surface

Fig.2 Time histories of horizontal displacements of observation points at (a) left boundary, and (b) free surface, under obliquely incident P wave with incidence angle $\theta = 60^{\circ}$

2.3 Calculation model

Considering a homogeneous, isotropic, and elastic half-space with a scarp topography (Fig.1). The elastic parameters are taken as: the shear wave velocity $v_s = 1000m/s$, the mass density $\rho = 1700kg/m^3$, and the poisson ratio $\mu = 0.25$. The calculation model and the observation points are shown in Fig.3, where point 1 are located at a distance of 100m from the left boundary, and the intervals from point 1 to point 17 are 40m. Smaller intervals of 20m are used from points 17-25. Along the slope, points 25-29 are equally spaced. The intervals of points 29-37 and points 37-53 are 20m and 40m, respectively. The distance from points 53 to the right boundary is 100m.

Assuming obliquely incident P waves from the left and right side of the model, and the incidence angle are defined as θ_1 and θ_2, respectively. The EL-Centro wave and the Ninghe wave are chosen as input waves, whose time histories are presented in Fig.4. To fulfill the accuracy requirement of the FEM, ten finite elements are contained in the shortest interested wavelength, and the mesh size is chosen as 5 m.

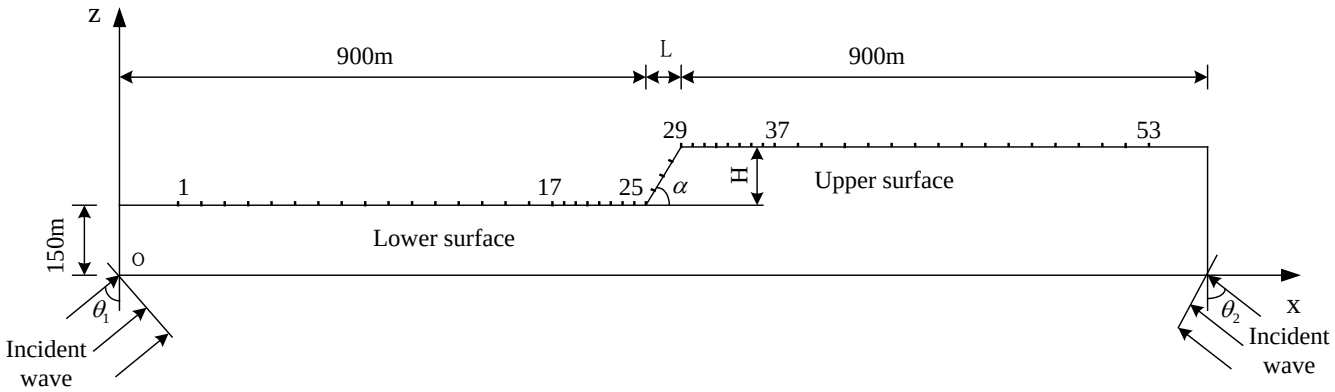

Fig.3 Scarp model and the observer's positions

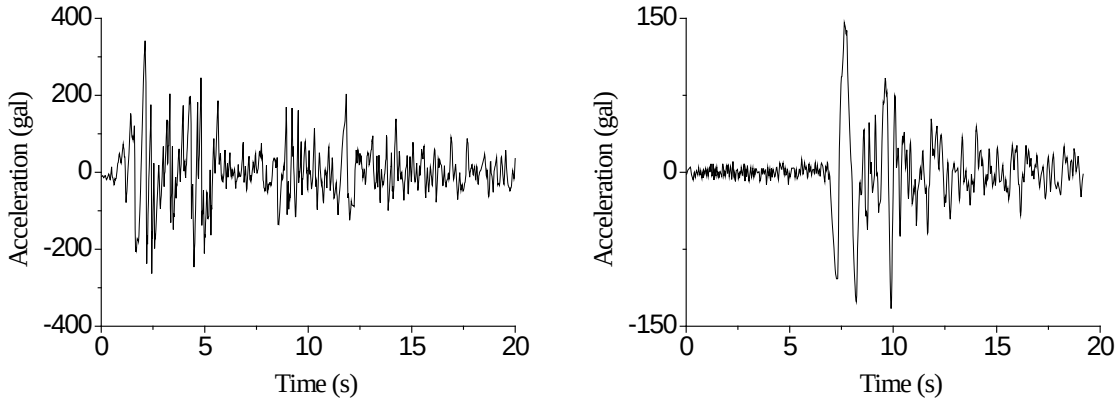

(a) EL-Centro wave (b) Ninghe wave

Fig.4 Acceleration time history of incident EL-Centro wave (left) and Ninghe wave (right)

3. Seismic response of free surface of scarp topography

Defining the seismic motion amplification factor (hereinafter referred to as amplification factor) β as the ratio of amplitude of free surface points, $A_{\max}$, to that of the input waves, $A_{\max,input}$, i.e., $\beta = \left| A_{\max} / A_{\max,input} \right|$. The amplification factor β is used in this study to quantify the amplification effect of scarp topography to the wave motion.

3.1 The effect of slope angle

Let the slope width of the scarp model L=60m, and plane P waves input from left and right side, respectively, with an incidence angle $\theta_1 = 30^\circ$. Fig.5~Fig.8 show the amplification factors of the free surface receivers for different incidence directions and incident waves. In each case the slope angle α equals to 0°, 10°, 20°, 30°, 40°, and 50°, respectively.

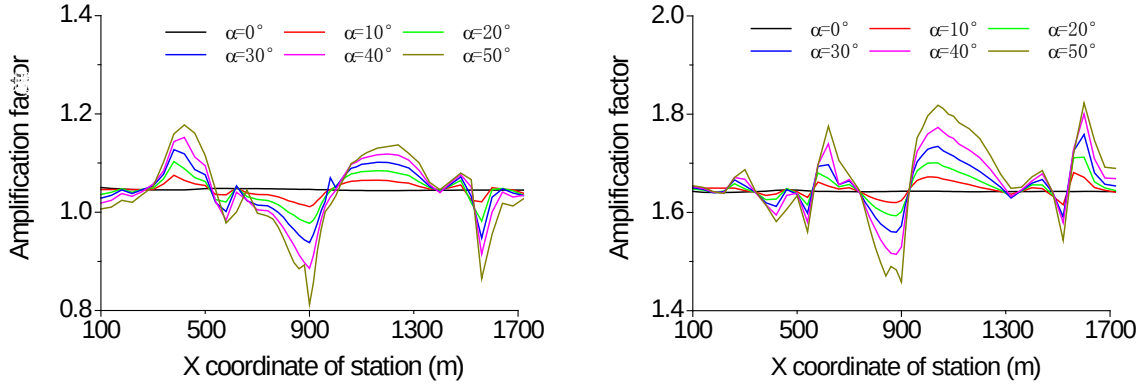

Fig.5 Amplification factors of surface points of scarp with left incident El-Centro wave and incidence angle $\theta_1 = 30^0$

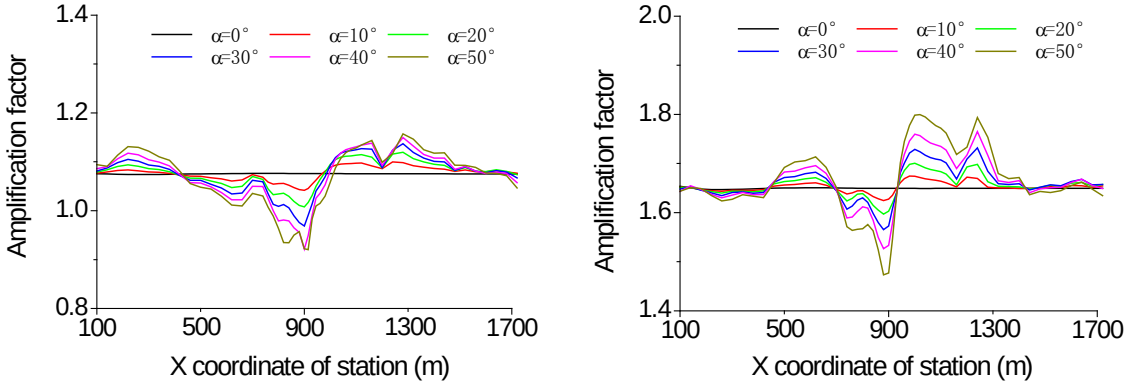

Fig.6 Amplification factors of surface points of scarp with left incident Ninghe wave and incidence angle $\theta_1 = 30^0$

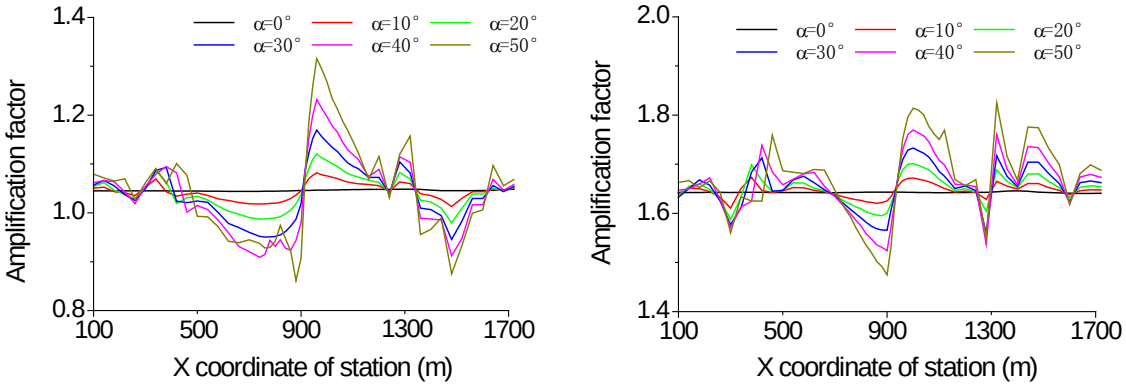

Fig.7 Amplification factors of surface points of scarp with right incident El-Centro wave and incidence angle $\theta_2 = 30^0$

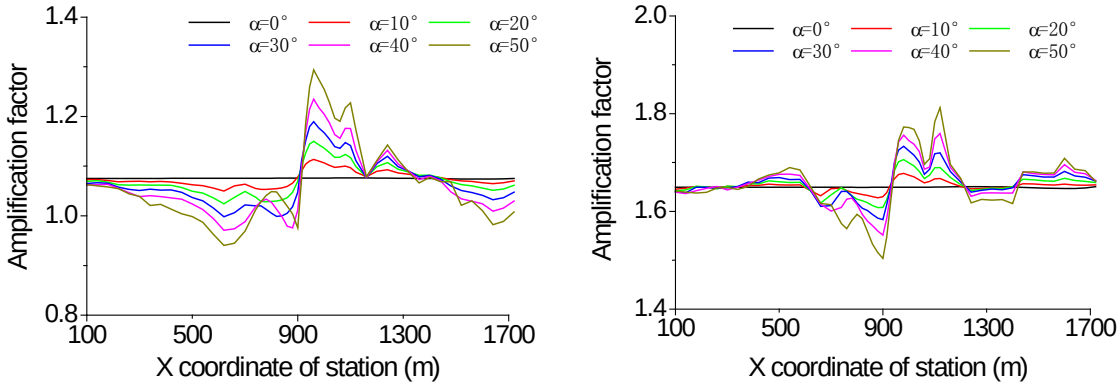

Fig.8 Amplification factors of surface points of scarp with right incident Ninghe wave and incidence angle $\theta_2 = 30^0$

It is shown in Fig.5 and Fig.6 that when P waves input from left side and incidence angle equals to 30°, for the x component, the amplification factors of the free surface points are all smaller than 2.0, and vary from 0.8 to 1.3, i.e., they are smaller than the free field value of vertical incidence case, which equals to 2.0 in theory. β of the upper surface is larger than the lower surface, and the maximal β does not occur at the top corner (point 29). In contrast, the distance to the top corner increases from 260m to 340m as the slope angle increases from 0° to 50°, and β decreases slowly after the maximum to a similar value at far positions. Additionally, β at the lower corner (point 25) is minimal, and it increases gradually from the lower corner to the top corner.

For the z component, β at the free surface points are all smaller than 2.0 as well, which varies from 1.4 to 1.8. β of the upper surface is larger than that of the lower surface, and the maximal β does not occur at the top corner (point 29). In contrast, the distance from the maximal β to the top corner increases from 120m to 160m as the slope angle increases from 0° to 50°. Additionally, β at the lower corner (point 25) is minimal, and it increases gradually from the lower to the top corner.

It is shown in Fig.7 and Fig.8 that when P waves input from right side and incidence angle equals to 30°, for the x component, the amplification factor of the free surface points varies from 0.8 to 1.3, and β of the upper surface is larger than that of the lower surface. The maximal β appears at the top corner (point 29), and the minimal β is found at the lower corner (point 25). Besides, β increases gradually from the lower corner to the top corner.

For the z component, the amplification factor of the free surface points varies from 1.4 to 1.8, and β of the upper surface is larger than that of the lower surface. The maximal β does not occur at the top corner (point 29), which is located at a distance of 120m from the top corner. The minimal β appears at the lower corner (point 25), and β increases gradually from the lower corner to the top corner.

These results show a general trend that the greater the slope angle, the larger the amplification factor of the top surface of the scarp model, and the smaller the amplification factor of the lower surface.

3.2 The effect of incidence angle

In this section, a constant slope angle of 45° is assumed, and a fixed slope height H and width L of 60m is considered. On this basis, the seismic responses of the scarp topography under different incident angles are investigated. Fig.9~Fig.12 give the amplification factors of the free surface receivers of scarp model under different incidence directions and incident waves. In each case the incidence angle θ equals to 0°, 10°, 20°, 30°, 40°, and 50°, respectively.

According to Fig.9 and Fig.10, when P waves input from left side and slope angle equals to 45°, for the x component, the amplification factors of the observation points are all smaller than 2.0, and increase with the growing of the incidence angle. The minimal β appears at the lower corner (point 25), but the maximal β does not occur at the top corner (point 29), and its location increasingly deviates from the upper edge with the growing incidence angle. The amplification factor has the minimal value for the vertical incidence case.

For the z component, it is shown that the smaller the incidence angle, the larger the amplification factor, and the closer the maximal β's position to the upper corner of the scarp. In contrast to the x component, the amplification factor has the maximal value for the vertical incidence case.

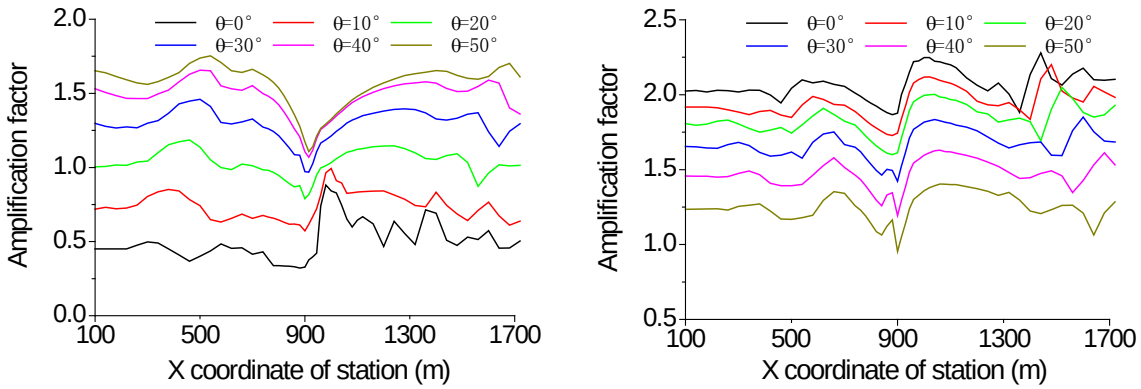

Fig.9 Amplification factors of surface points of scarp with left incident El-Centro wave and slope angle $\alpha = 45^0$

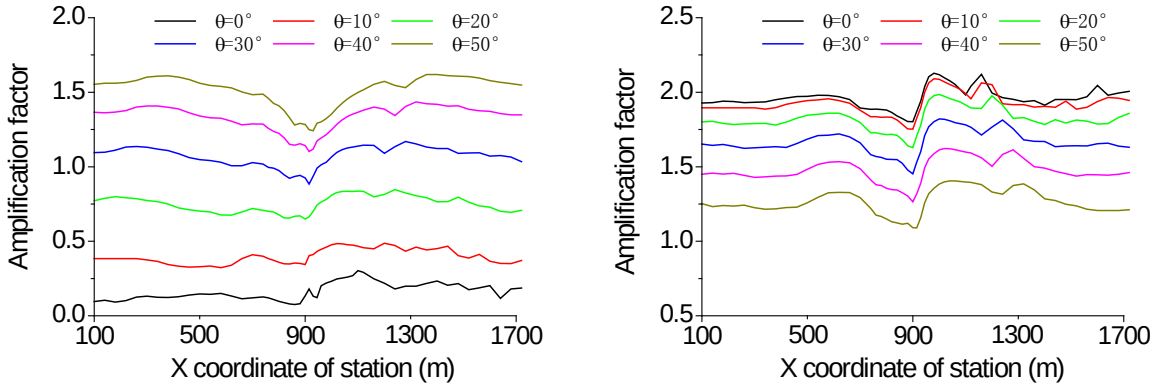

Fig.10 Amplification factors of surface points of scarp with left incident Ninghe wave and slope angle $\alpha = 45^0$

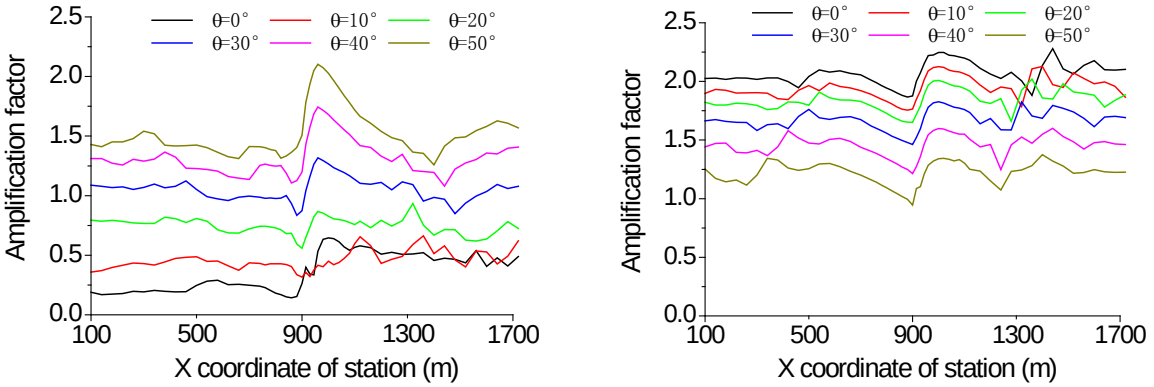

Fig.11 Amplification factors of surface points of scarp with right incident El-Centro wave and slope angle $\alpha = 45^0$

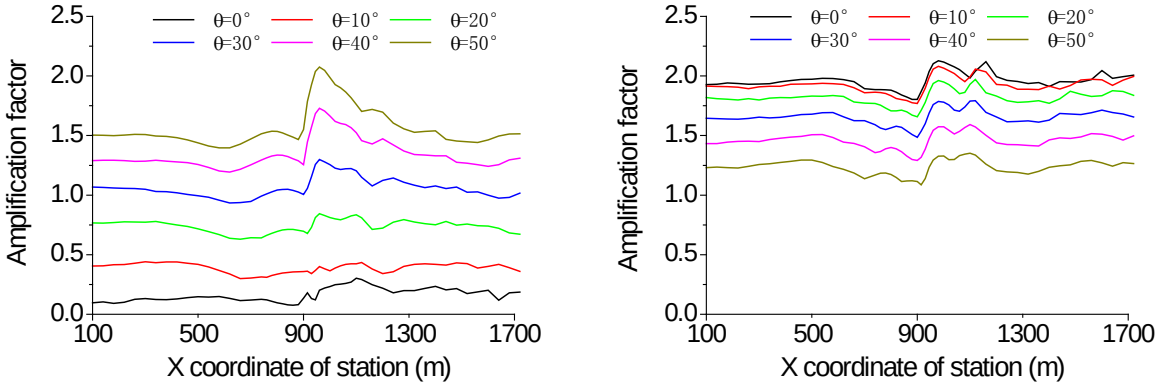

Fig.12 Amplification factors of surface points of scarp with right incident Ninghe wave and slope angle $\alpha = 45^0$

According to Fig.11 and Fig.12, when P waves input from right side and slope angle $\alpha = 45^\circ$, for the x component, the amplification factor increases with the growing of the incidence angle. Beyond a certain value of the incidence angle, β of the upper surface will exceed 2.0, and the position of the maximal β becomes more and more close to the top corner (point 29). For each case, the minimal β appears at the lower corner (point 25). And in general, the amplification factor has the minimal value for the vertical incidence case.

For the z component, it is shown that the smaller the incidence angle, the larger the amplification factor, and the closer the maximal β's position to the upper corner of the scarp. The amplification factor shows the maximal value for the vertical incidence case. Compared with the left incidence case, the influenced range of the upper surface of the scarp becomes smaller.

3.3 Comparison with the results of SV wave incidence

Considering the slope angle $\alpha = 50^{\circ}$, the slope width L=60m, and left side incident seismic waves with an angle of 30°. Fig.13 and Fig.14 compare the amplification factors of the free surface points of scarp model when the input wave is El-Centro wave and Ninghe wave, respectively. In each case, the input wave is in the form of P wave and SV wave, respectively.

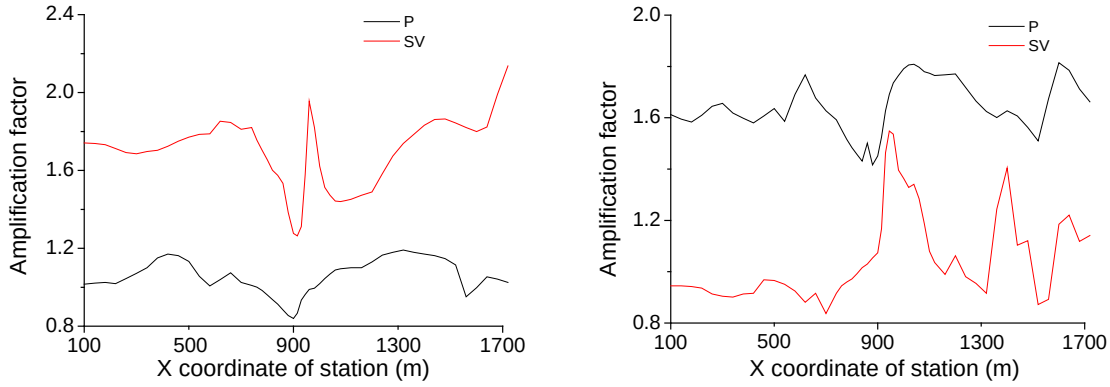

Fig.13 Amplification factors of surface points of scarp with 30° left incident El-Centro wave and slope angle $\alpha = 50^{\circ}$

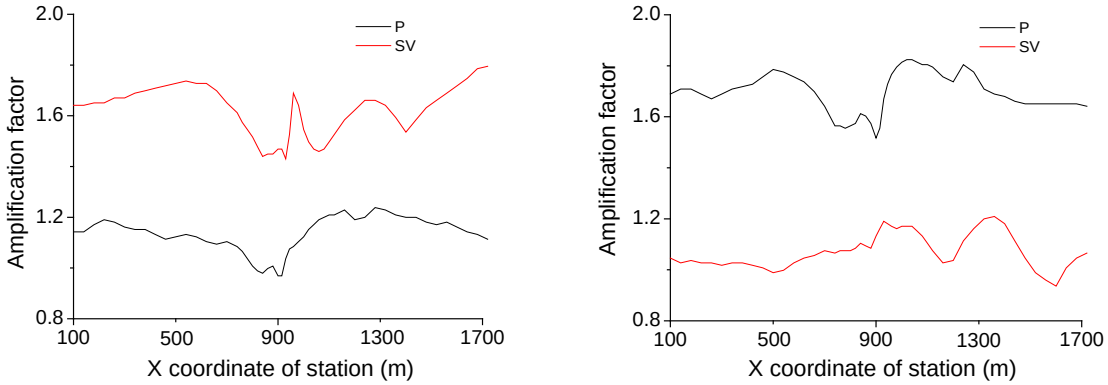

Fig.14 Amplification factors of surface points of scarp with 30° left incident Ninghe wave and slope angle $\alpha = 50^{\circ}$

Compared with P wave incidence case, the seismic response amplitudes of the x component are larger than that of the z component when the input wave is SV wave. Besides, the distribution characteristic of the amplification factor is similar to the findings of Ashford and Sitar (1997). However, due to the difference of the calculation model, such as the damping effect and the higher frequency of the input wave, which were considered in the latter, the amplitudes of the amplification factor are different for the two studies.

4. Conclusions

In this study, seismic effect of scarp topography under inclined P waves is investigated by using the numerical method, and the effects of incidence angle, the slope angle, and the incident direction on the propagation of seismic waves are analyzed, respectively. The following conclusions can be drawn:

(1) The influenced extent and range to the ground motion amplification factor has a little difference for different input waves, such as the El-Centro wave and the Ninghe wave, but the trend is similar. In addition, the influenced trend of oblique incidence case is more complex than that of the vertical incidence case, which is also found by other studies.

(2) The amplification factor gradually increases from the lower corner to the top corner of the scarp, which is not affected by the incidence angle, the slope angle, and the incident direction.

(3) When the incidence angle is constant, the amplification factor at the upper surface is larger than that of the lower surface, which is not affected by the incidence direction. Meanwhile, the amplification factor increases with growing slope angle.

(4) When the slope angle is constant, and the waves input from left side, the amplification factor of x component increases with growing incidence angle, while the opposite is true for the z component.

(5) When waves input from left side, the maximal amplification factor does not occur at the top corner of the scarp, and the deviation becomes larger with increasing slope angle. Additionally, the deviation of x component is larger than the z component. When waves input from right side, the maximal amplification factor is generally located at the top corner of the scarp, especially for the x component. No matter what case, the minimal amplification factor can always be found at the lower corner.

(6) Compared with right incidence case, the x component amplification factor is larger for left incidence case, but the z component amplification factor is not sensitive to the incident direction.

(7) Both horizontal and vertical ground motions will occur at the free surface for inclined P-wave and SV-wave, respectively. However, for P wave incidence case, ground motion amplitudes of z component is larger than that of x component, and the opposite occurs for the SV wave incidence case.

5. Acknowledgements

This research is supported by the National Natural Science Foundation of China under Grant No. 51278323.

6. References

[1] Y-X. Hu, S-C. Liu and W. Dong (1996). *Earthquake Engineering*, London: E & FN SPON.

[2] Davis LL, West LR (1973): Observed effects of topography on ground motion. *Bulletin of the Seismological Society of America*, **63** (1), 283-298.

[3] Clough RW, Chopra AK (1966): Earthquake stress analysis in earth dams. *Journal of the Engineering Mechanics Division*, **92** (2), 197- 212.

[4] Li X, Zhou Z, Yu H, et al (2008). Strong motion observations and recordings from the great Wenchuan Earthquake. *Earthquake Engineering and Engineering Vibration*, **7**(3): 235-246.

[5] Trifunac MD (1973): Scattering of plane SH-waves by a semi-cylindrical canyon. *Earthquake Engineering and Structure Dynamics*, **1** (3), 267-281.

[6] Wong HL, Trifunac MD (1974): Scattering of plane SH-waves by a semi-elliptical canyon. *Earthquake Engineering and Structure Dynamics*, **3** (2), 157- 169.

[7] Trifunac MD (1971) : Surface motion of a semi-cylindrical alluvial valley for incident plane SH waves. *Bulletin of the Seismological Society of America*, **61** (6), 1755- 1770.

[8] Wong HL, Trifunac MD (1974) : Surface motion of a semi-elliptical alluvial valley for incident plane SH waves. *Bulletin of the Seismological Society of America*, **64** (5), 1389-1408.

[9] Cao H, Lee VW (1989) : Scattering of plane SH-waves by circular cylindrical canyons with variable depth-to-width ratio. *European Earthquake Engineering*, **2**: 29-37.

[10] Yuan X, Liao Z P (1994). Scattering of plane SH waves by a cylindrical canyon of circular-arc cross-section. *Soil Dynamics and Earthquake Engineering*, **13**(6): 407-412.

[11] Todorovska M, Lee VW (1991) : Surface motion of shallow circular alluvial valleys for incident plane SH waves: analytical solution . *Soil Dynamics and Earthquake Engineering*, **10** (4), 192-200.

[12] Lee V W, Sabban M A, Ghosh T K (1995). 3-D surface motions of long semi-circular longitudinal canyons I: Incident plane P waves. *European Earthquake Engineering*, **9**(3): 12-22.

[13] Ashford SA, Sitar N (1997): Analysis of topographic amplification of inclined shear waves in a steep coastal bluff. *Bulletin of the Seismological Society of America*, **87** (3), 692–700.

[14] Ashford SA, Sitar N, Lysmer J, et al. (1997): Topographic effects on the seismic response of steep slopes. *Bulletin of the Seismological Society of America*, **87** (3), 701–709.

[15] Zhao M, Du X, Liu J, et al (2011). Explicit finite element artificial boundary scheme for transient scalar waves in two-dimensional unbounded waveguide. *International Journal for Numerical Methods in Engineering*, **87**(11): 1074-1104.

[16] Liao Z P, Wong H L, Yang B P, et al (1984). A transmitting boundary for transient wave analysis. *Scientia Sinica*, **27**(10): 1063-1076.

[17] Liao Z P, Wong H L (1984). A transmitting boundary for the numerical simulation of elastic wave propagation. *Soil Dynamics and Earthquake Engineering*, **3**(4): 174-183.